Journal of Metals, Materials and Minerals, 33(4), 1624, 2023

Structure and chemical durability improvement of alkali silicate glass by zirconium dioxide and erbium oxide addition

Ativit DENPRAWAT[1], Kittipong SINWANASARP[1], Pinit KIDKHUNTHOD[2], Nattapol LAORODPHAN[3], and Worapong THIEMSORN[1,*]

[1] *Department of Industrial Chemistry, Faculty of Science, Chiang Mai University, Muang District, Chiang Mai, 50200, Thailand*
[2] *Synchrotron Light Research Institute (Public Organization), Muang District, Nakhon Ratchasima, 30000, Thailand*
[3] *Department of Industrial Chemistry Innovation, Faculty of Science, Maejo University, San Sai District, Chiang Mai, 50290, Thailand*

***Corresponding author e-mail:** worapong.t@cmu.ac.th

Received date:
6 February 2023
Revised date
15 September 2023
Accepted date:
1 November 2023

Keywords:
Chemical durability;
Charge compensator;
X-ray absorption spectroscopy;
Glass structure;
Rare earth oxide containing glass

Abstract

Glass structure tailoring of alkali silicate glasses by addition of ZrO_2 and Er_2O_3 is found to enhance the chemical durability of glasses. ZrO_2 (x ranged between 5 mol% to 15 mol%) and Er_2O_3 (y ranged between 0.5 mol% to 1.5 mol%) were used to replace SiO_2 and Na_2O, respectively, in the glasses with the nominal composition of $10Li_2O$-(15-y)Na_2O-10CaO-(65-x)SiO_2-xZrO_2-y Er_2O_3. The samples were prepared by conventional melt quenching technique. The structures of produced glasses were examined by X-ray absorption spectroscopy (XAS) and Raman spectroscopy. XAS spectra demonstrated that the oxidation numbers of Zr and Er ions were +4 and +3, respectively. The chemical environment around both cations was six-fold coordination. In addition, Raman spectra demonstrated that the Zr^{4+} ions formed the Q^4(Zr) structure, which caused the reduction of non-bridging oxygen. In case of the Er^{3+} ions, the formation of the Si-O-Er bonds was explained from the Raman study. The chemical durability of glass was determined from Na^+ ions leaching values. In pH 7 solution, the leached Na^+ ions reduced from 25.67% to 21.43% and from 22.50% to 20.49% as a function of concentration of ZrO_2 (x = 5 mol% to 15 mol%) and Er_2O_3 (y = 0.5 mol% to 1.5 mol%), respectively. As the results, the chemical durability of the ZrO_2-containing and Er_2O_3-containing glasses were significantly improved due to charge compensated mechanism and enhancing network rigidity by increasing cation field strength. Moreover, the micro-hardness (580 HV to 837 HV) and density (2.54 g·cm^{-3} to 2.82 g·cm^{-3}) also displayed an increased tendency with larger concentration of ZrO_2 and Er_2O_3.

1. Introduction

Nowadays, soda-lime-silicate glasses are important commercial materials for producing building materials, and food and beverage containers due to their excellent chemical durability [1]. However, soda-lime-silicate glasses can gradually interact with moisture in the atmosphere and aqueous solutions, which chemical reaction will generate thin white film or white crystalline solid depositing on the glass surface [2]. The film or solid can often be removed by washing; nevertheless, the smoothness and transparency of the glass after washing are reduced [3]. In principle, soda-lime-silicate glasses are composed of relatively high sodium ion content (Na^+), especially on glass surface. These free Na^+ ions reportedly relate to the chemical weathering reaction on the glass surface [4].

In the past, there are a lot of techniques to avoid or slow down degradation processes occurring on glass surface, such as, the increasing amount of silica and/or alumina, reducing the mobility of alkali ions, reducing the concentration of alkali ions on the surface, and creating the barrier coats to retard the contact of fluid to the glass surface [5]. In this work, the technique that diminishes the mobility of the alkali ions by doping heavy metal oxide (transition metals or rare earths) was selected. Various transition metal oxides and rare earth oxides, for example Fe_2O_3 [6], SnO_2 [7], ZnO [8], Nd_2O_3 and Gd_2O_3 [9], were doped into a glass matrix in order to reduce the corrosion, leaching, weathering, and chemical reactions, resulting in a greatly extended useful life.

Zirconium oxide (ZrO_2) has been found to significantly modify the physical properties of alkali silicate glasses, such as increase the density, viscosity, glass transition temperature, and decrease the thermal expansion coefficient [10-13]. Moreover, ZrO_2 has been reported to improve chemical resistance of alkali silicate glasses in water, acid, and basic solutions. For example, addition slight amount of ZrO_2 in soda-lime silicate glasses significantly decrease dissolution rate of glasses in distilled water [11]. Moreover, it was reported that the dissolution rate under very corrosive environment for long period of time decreases significantly with doping ZrO_2 in soda lime borosilicate glasses [14]. The improvement in the chemical durability from ZrO_2 can be relative with the structural changes. When Zr^{4+} ions associate into the glass structure as $[ZrO_6]^{2-}$ octahedra, each conner of them prefer to link with $[SiO_4]^{4-}$ tetrahedra; moreover,

the negatively charged surplus of $[ZrO_6]^{2-}$ octahedra is stabilized by the charge compensator (alkali or alkaline earth ions) which has been confirmed that its ionic mobility is enormously lower than the network modifier [15-19].

The addition of rare earth oxides in the glass structure were found to be effective ways to modify various glass properties [20-23]. The fundamental function of rare earth oxides in glass is modifier since the behavior of rare earth oxides is like other modifier oxides [15, 24-28]. However, rare earth ions have higher field strength than alkali or alkaline earth ions, which the cations tend to be easily incorporated in the glass network at non-bridging oxygen region and produce tighter structures [15,29-31]. In addition, rare earth can transform the lower field strength cations from the modifier to the charge compensator to satisfy their environment [15,29,30]. Therefore, rare earth oxides can be used to enhance chemical durability of glass.

Herein, we investigated the effect of chemical tailoring of glasses on the structure and chemical durability of glasses together with their hardness and density. The chemical composition changing was done by SiO_2 and Na_2O replacement with ZrO_2 and Er_2O_3, respectively. Raman spectroscopy and synchrotron-base X-ray absorption spectroscopy were applied to study the structure of glasses. Vicker microhardness of the ZrO_2 and Er_2O_3 containing glasses and the glass densities were also compared. The percentage of Na^+ ion leaching from the glass represents the chemical durability of glasses in this study following the ASTM C1285-21 standards.

2. Experimental

2.1 Glass preparation

The starting alkali silicate glass was prepared using Li_2CO_3, Na_2CO_3, $CaCO_3$ and SiO_2 as starting materials by conventional melt quenching technique. ZrO_2 was replaced the amount of SiO_2 to obtain the batch glasses in $10Li_2O$-$15Na_2O$-$10CaO$-$(65-x)SiO_2$-$xZrO_2$ system, where x = 0, 5, 10, and 15 mol%. These glasses were then indicated as Zr0, Zr5, Zr10, and Zr15, respectively. The homogeneous mixtures giving 100 g of glasses were placed into an alumina crucible. The batches were heated at 1400°C for 130 min in an electrical furnace with the heating rate of 10°C·min^{-1}. The glass melts were rapidly shaped by pouring into a stainless steel mold, then annealed at 570°C for 2 h, and finally cooled down to room temperature. As a result of Na^+ ions leaching and formability, the Zr5 glass was selected as the based glass for Er_2O_3 study. The Na_2CO_3 was partially substituted by Er_2O_3 in order to obtain $10LiO_2$-$(15-y)Na_2O$-$10CaO$-$60SiO_2$-$5ZrO_2$-yEr_2O_3 glasses where y = 0, 0.5, 0.75, 1.0, 1.25 and 1.5 mol%. The glasses were indicated as Zr5Er0, Zr5Er0.5, Zr5Er0.75, Zr5Er1.0, Zr5Er1.25, and Zr5Er1.5, respectively. These glass batches were prepared using the same condition.

2.2 Structural characterization

The glass samples were ground using a mortar and then sieved through a 200-mesh screen to control particle size. The fine powder was characterized by an X-ray diffractometer (Rigaku Co., Tokyo, Japan) with CuKα radiation operating at room temperature to confirm the phase composition. Diffraction pattern was collected at the 2θ scanning range of 5° to 60° with step size of 0.01° and scanning rate 10°·min^{-1}.The diffraction patterns were analyzed using Qualx software.

Raman spectroscopy measurements of the glass samples were carried out to identify the chemical bond, the proportion and type of oxygen in glass structure, whether it is bridging oxygen (BO) or non-bridging oxygen (NBO). The Raman spectra were acquired using LabRAM HR Evolution spectrometer with an excited laser wavelength of 532.13 nm and 150 mW power for 30 s.The measurement range was in 100 cm^{-1} to 2000 cm^{-1} with 3 repetitions. The Raman spectra were also fitted.

Synchrotron-based XAS experiment was conducted at the SUT-NANOTEC-SLRI XAS Beamline (BL5.2), Synchrotron Light Research Institute (Public Organization), Thailand. The X-ray absorption near edge structure (XANES) and extended X-ray absorption fine structure (EXAFS) analysis were used to characterize the oxidation states and local structure around Zr and Er atoms. Zr and Er L-edge spectra were collected in the fluorescence modes. The XAS data were processed and normalized using Athena software. EXAFS data were also analyzed using Artemis software.

2.3 Measurements of glass properties

The densities of glass samples were calculated by the Archimedes principle that an electronic balance (Sartorius, BSA224S-CW) was employed for mass measurements. This method relies on weighing the glass sample in both a liquid (W_{liq}) and in air (W_{air}). The bulk densities of glass samples were determined using Equation (1).

$$\text{Bulk density (g·cm}^{-3}) = \rho_{liq} \frac{W_{air}}{W_{air} - W_{liq}} \quad (1)$$

Where, W_{air} is weight of sample measured in air, W_{liq} is weight of sample measured in liquid, and ρliq is density of liquid.

The microhardness was measured in a perpendicular direction with the surface of the glass samples. The measurement was performed by a Vicker microhardness tester (GALILEO-durometria). Vicker indentations were performed using loads up to 1000 g pressing on surfaces of samples for 15 s. Vicker microhardness number (HV) could calculate by the relation shown in Equation (2).

$$HV = 1.8544 \times \left(\frac{P}{d^2}\right) \quad (2)$$

where, HV is the Vicker microhardness number, P is the applied load and d is the average diagonal length of the indentation mark.

To evaluate the chemical durability of the glass sample, the test was performed based on the leaching test standard (ASTM C1285-21). Prior to the measurements, the glass samples were grounded using a zirconia grinding ball and sieved through a 325-mesh screen to control particle size. The glass powder was immersed in deionized water (pH 7), acid (HCl, pH 2) and alkaline (KOH, pH 10) solutions, using the same ratio of powder to solution at 1 g to 10 cm^{-3}. The leaching experiments were carried out in a high-density polyethylene (HDPE) container placed in an electrical oven at 90°C for 7 days. In the end, the basic, acidic, and neutral leaching solutions were analyzed to detect the concentration of leached Na^+ ions from glass powder by Flame photometer (Sherwood-410). The percentage of leached Na^+ ions from

bulk glass comparing to the nominal sodium content could be calculated by the relationship shown in Equation (3).

$$\text{The percentage of leached } Na^{+} \text{ ions } = \frac{W_S}{W_P} \times 100 \qquad (3)$$

where, W_s is weight of Na element in solution, W_p is weight of Na element in glass powder.

3. Results and discussion

3.1 Phase analysis

All compositions were completely melted and formed transparent glass samples as shown in Figure 1(a) and Figure 1(b) for ZrO_2 and Er_2O_3 studies, respectively. The XRD patterns of the based glass (Zr0) and Zr-doped glasses (Zr5, Zr10 and Zr15) display in Figure 2(a). The results reveal a broadened peak and weak intensity with 2θ centered at range of 26°to 28° that is characteristic diffraction pattern of amorphous structure [20].

The XRD patterns of the glasses doped with Er_2O_3 0.5, 1.0 and 1.5 mol% (Zr5Er0.5, Zr5Er1.0 and Zr5Er1.5) display in Figure 2(b). The diffraction patterns reveal no obvious peaks or lines associated with any crystalline phase. These XRD patterns can confirm that Er_2O_3 is dissolved in glass matrix homogeneously.

3.2 Analysis of Raman spectra

Raman spectra of Zr0, Zr5, Zr10, and Zr15 glasses are shown in Figure 3 in the 100 cm^{-1} to 1500 cm^{-1} range. The spectra can be divided into two regions that comprise low frequency region (100 cm^{-1} to 800 cm^{-1}) and high frequency region (800 cm^{-1} to 1300 cm^{-1}), which involve the types of vibrational mode of Si-O bonds [30,32-34]. The low frequency region relates to the vibration in rocking and bending mode of the Si-O bonds and their tetrahedral cations, while the high frequency region corresponds to the vibration in stretching mode of Si-O bonds within tetrahedral site. The high frequency region also gives important information to identify types of silicon tetrahedra structural units Q^n (n = number of bridging oxygen), referring to the degree of connectivity in glasses. The Zr0 glass reveals the peak around 590 cm^{-1} corresponding to Si-O-Si bending vibration in glass network disconnectivity [35]. When increasing concentration of ZrO_2, the peak positions are altered depending on ZrO_2 content. The peak shifts towards higher wavenumber near 610 cm^{-1} (Zr5) and split into two peaks near 540 cm^{-1} and 630 cm^{-1} (Zr10 and Zr15), respectively [36].

Raman spectra in high frequency region are fitted with Gaussian distribution model for 3 peaks at 950, 1030 and 1070 cm^{-1} as shown in Figure 4(a-d) [32,34]. For the Zr0 glass, 3 peaks are assigned as the stretching vibration of Si-O within $[SiO_4]^{4-}$ unit. The peak near 950 cm^{-1} corresponds to the Si-O stretching of $[SiO_4]^{4-}$ units with two non-bridging oxygen; NBOs (Q^2). The two peaks near 1030 cm^{-1} and 1070 cm^{-1} are due to the Si-O stretching within $[SiO_4]^{4-}$ units with one NBO (Q^3) site. The peak positions depend on type of cations bonding with NBOs. The peaks around 1030 cm^{-1} and 1070 cm^{-1} correspond to the bonding of NBOs with calcium ion (Q^3(Ca)) and sodium ion (Q^3(Na)), respectively [32]. When ZrO_2 was added, there are observable changes in peak intensities, especially, near 950 cm^{-1} and 1070 cm^{-1}.

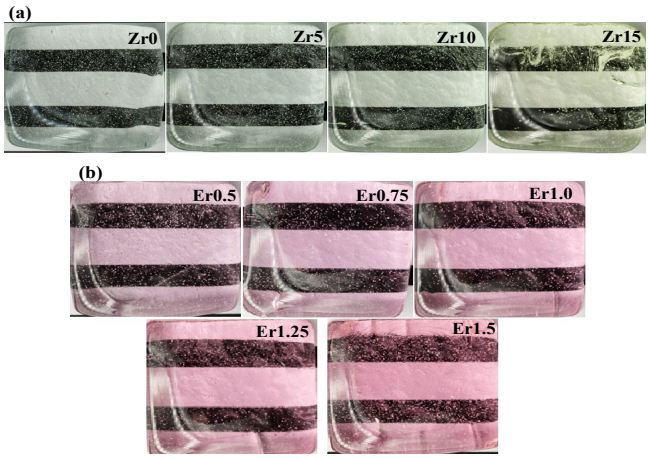

Figure 1. The doped glass samples with different concentrations of (a) ZrO_2 and (b) Er_2O_3

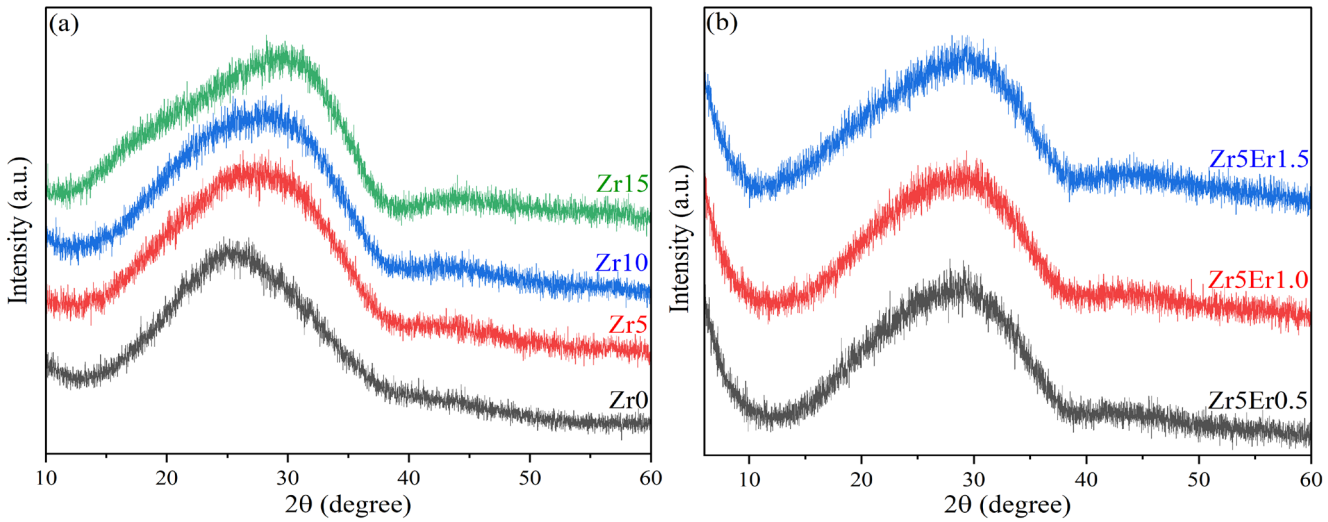

Figure 2. XRD diffraction patterns of (a) glasses containing different ZrO_2 concentrations and (b) glasses containing different Er_2O_3 concentrations.

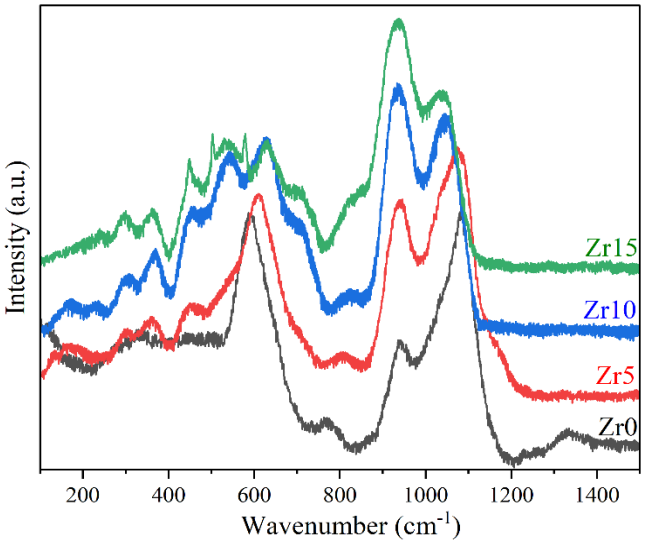

Figure 3. Raman spectra of Zr0, Zr5, Zr10, and Zr15 glasses.

The peak intensity around 1070 cm^{-1} decreases, while the intensity of the band around 950 cm^{-1} is reversed with increasing ZrO_2 concentration. The growing peak near 950 cm^{-1} is assigned to a stretching mode within $[SiO_4]^{4-}$ unit connecting with two $[ZrO_6]^{2-}$ octahedra (Q^4(Zr,Zr)) or the $[SiO_4]^{4-}$ units may be connected to both $[ZrO_6]^{2-}$ unit and Na^+ ion (Q^3(Zr,Na)) [15,36]. On the other hand, the intensity of peak, especially, near 1070 cm^{-1} has an invert relationship with concentration of ZrO_2 and finally diminished when ZrO_2 concentration achieve 15 mol%. This tend relates with electronic structure of $[ZrO_6]^{2-}$ unit, in which each Zr atom generates two negative charge surplus (-2). Consequently, charge compensators need for stabilizing the negative charge surplus of $[ZrO_6]^{2-}$ unit that Na^+, Li^+ and Ca^{2+} ions are excellent choice. Na^+ ions has been reported that it prefers being a charge compensator more than the Ca^{2+} ions [15]. The proportions of relative intensities of tetrahedron structural units (Q^n) and the ZrO_2 concentration are shown in Figure 5. The percentage of Q^3(Na) decreases severely than Q^3(Ca) because role of Na^+ ions at non-bridging oxygen site converts from network modifier to be charge compensator near $[ZrO_6]^{2-}$ unit.

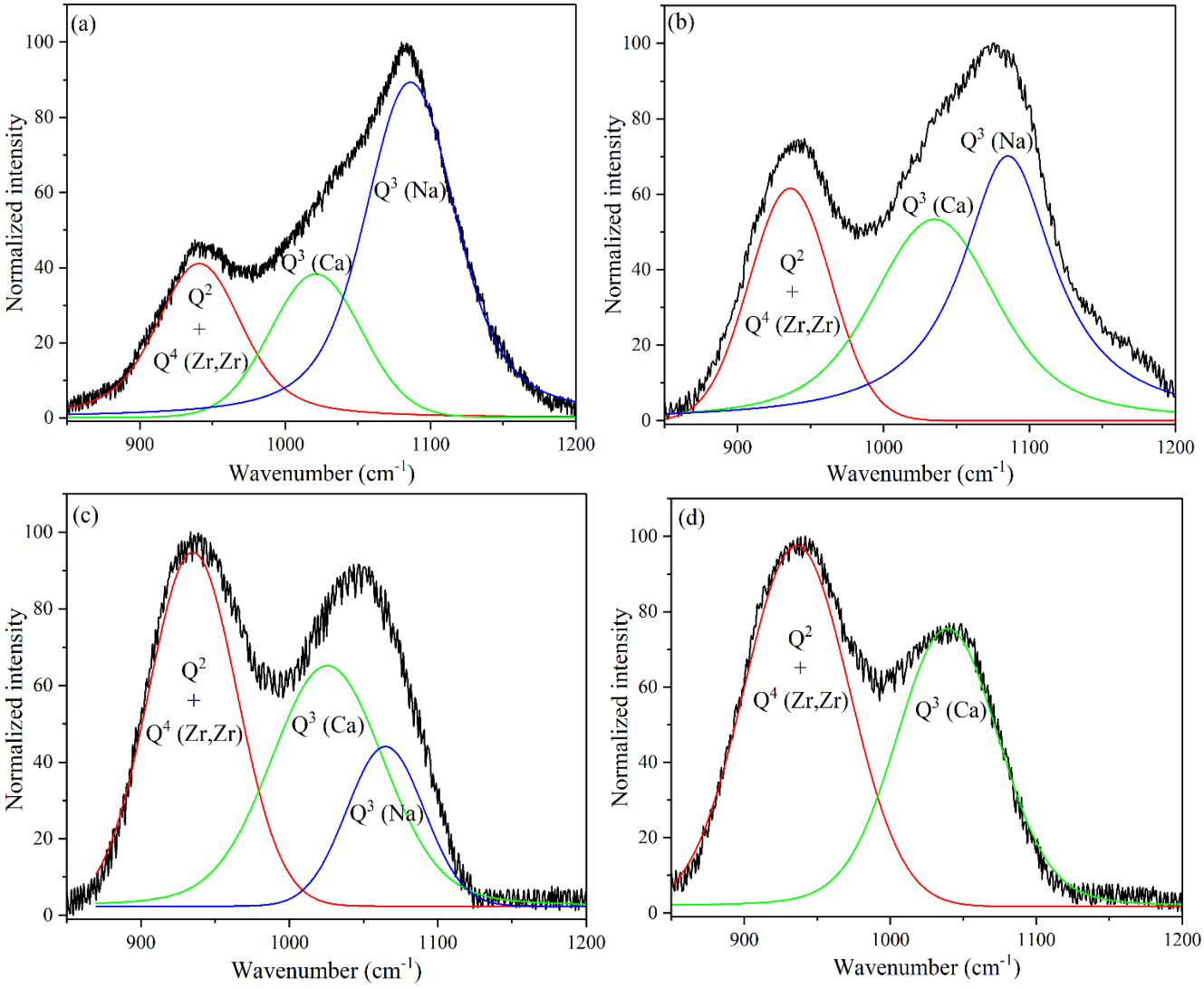

Figure 4. Fitting of Raman spectra of (a) Zr0, (b) Zr5, (c) Zr10, and (d) Zr15 samples.

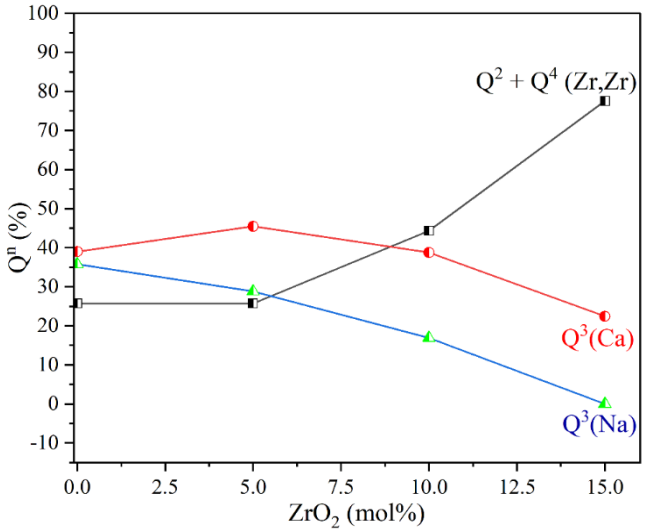

Figure 5. Relative concentration of different structural units of silicon tetrahedra (Q^n) according to the fitting of the Raman spectra shown in Figure 4.

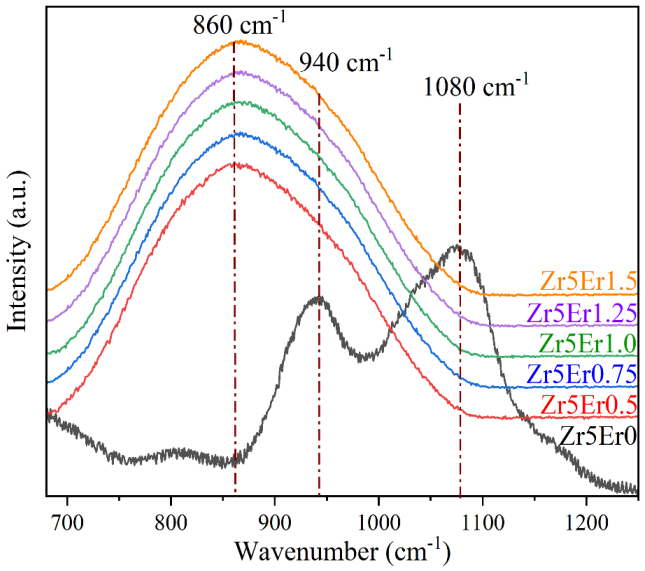

Figure 6. Raman spectra of glasses containing different Er_2O_3 concentrations.

The Raman spectra of Zr5Er0, Zr5Er0.5, Zr5Er0.75, Zr5Er1.0, Zr5Er1.25, and Zr5Er1.5 glasses are illustrated in Figure 6. The results show the dramatic change of Raman spectra of Er_2O_3 doped glasses. This change was also clearly reported in MoO_3 doped glasses (0 mol% to 2 mol%), which has dominated Raman peak at 916 cm^{-1} [37]. It is indicated that rare earth oxides, such as MoO_3 (0 mol% to 1.67 mol%), Nd_2O_3 (0 mol% 3.77 mol%), RuO_2 (0 mol% to 1.01 mol%), has strong impact on glass structure [38]. The Er^{3+} ion significantly affects to reduce the intensity of peak around 1000 cm^{-1} to 1100 cm^{-1} and 950 cm^{-1}, whereas a new peak emerges at approximately 860 cm^{-1}. The peaks are produced by the vibrational modes of Si-O bonds within $[SiO^4]^{4-}$ tetrahedra that coordinate with Er^{3+}, Na^+, Li^+ or Ca^{2+} ions. There are two assumptions that could explain the transformation in Raman spectra when Na^+ ions are replaced with Er^{3+} ions. First, the shift to lower frequency in the spectra suggests that the angle between the Si-O-Si bonds decreases and the vibrations of the bridging oxygen become more distorted structure [35]. This implies that Er_2O_3 acts as a modifier in the silicate glass network, decreasing the degree of connectivity by increasing the concentration of NBOs [26,27,30]. From Table 1, Er_2O_3 will also be considered as network modifiers (SM-O < 0.75) according to previous work [39]. Moreover, several studies have also found that rare earth cations tend to be located in areas of the $[SiO_4]^{4-}$ unit where the connectivity has been reduced. In these areas, the rare earth cations can find both oxygen anions to complete their coordination number and alkali or alkaline earth cations to balance the excess negative charge from the polyhedral structure [15,25,27,28,30,40]. Second, a more probable hypothesis is that the shift in the lower frequency of Raman spectra is not correlated with an increase in the number of NBO sites. The Q^2 and Q^3 still exist in the glass structure as well as the based glass, while Q^1 does not occur. The shift in peak position is due to the change of symmetric stretching frequency of the $[SiO_4]^{4-}$ tetrahedron when its NBOs coordinate with high valence cations. For example, in sodium silicate glasses, the peak position for the Q^3 species is typically found at 1100 cm^{-1} [41]. However, when the Na^+ ions are replaced with Ca^{2+} ions in calcium silicate glasses, the peak position shifts to near 1070 cm^{-1} [32,41]. The peaks associated with the same species (Q^3) that coordinate with Ca^{2+} ion have a lower frequency because of the bond energy between the NBO and cation. According to complete neglect of differential overlap (CNDO) molecular orbital calculations, the strength of the Si-NBO bond decreases as the bond energy between the NBO and cation increases. This is indicated by a decrease in the Si-NBO force constants and corresponding vibrational peaks [42,43]. This study suggests that the bond energy of the NBO-M bond has a direct impact on the strength of the Si-NBO bond in inverse relation. With this assumption, the Er^{3+} ion associates with NBOs in the same position as an alkali or alkali earth cation, the peak position of the Raman spectrum for glasses containing Er^{3+} ions should shift to a lower frequency compared to the base glass. This is because the bond energy of the Er-NBO bond is greater than the bond energy of the alkali/alkali earth cation, resulting in a lower frequency for the Raman peaks.

Table 1 Diatomic distance, bond energy, and bond valence between various cations and oxygen.

Bonds	**d (M-O) (Å)**	**Bond energy ($kJ \cdot mol^{-1}$)**	**Bond valence (S_{M-O})**
Li-O	1.95	340.5	0.27
Na-O	2.38	270	0.21
Ca-O	2.48	383.3	0.25
Er-O	2.32	606	0.41
Zr-O	2.08	766.1	0.68
Si-O	1.68	799.6	1.01

3.3 XANES and EXAFS analysis

Figure 7(a) shows Zr L_{III} XANES spectra of standard reference compound; ZrO_2 (baddeleyite; Zr^{4+}), and Zr5, Zr10, and Zr15 glasses. The intensity of spectra increases along the concentration of ZrO_2. The first peak position of the samples at lower energy appears at 2227.21 ± 0.006 eV, which is very close to the one of reference compound, i.e., ZrO_2, at 2227.29 eV (Table 2). Therefore, the XANES data can confirm that the oxidation state of Zr atoms in all of glass samples is still +4. Moreover, the sharps of the Zr L_{III} XANES spectra also correspond to the site symmetry and coordination number of Zr atom [17,44]. The ZrO_2 (baddeleyite) that is coordinated by seven oxygen atoms has a boarded single absorption peak. Whereas Zr L_{III} XANES spectra all of glass samples exhibit double peaks (doublet) at the top of the absorption.The doublet has been identified as characteristic of Zr atom in six-fold coordination [17,36,44]. According to crystal field theory, the energy level of the 4d orbital of Zr atoms can be split into e_g orbitals (higher energy) and t_{2g} orbitals (lower energy) in association with six ligands arrangement. Activated electrons in L shell by X-ray, can relocate to both eg and t_{2g} orbitals [45]. The average of apparent crystal field splitting value from this experiment is 3.08 ± 0.01 eV. Thus, the characteristic of spectra also helps confirm the local environment of Zr atom in glass structure in this research that it is in octahedral coordination site.

Figure 7(b) shows Zr L_{III} XANES spectra of Er_2O_3 containing glasses, i.e. Zr5Er0.5, Zr5Er0.75, Zr5Er1.0, Zr5Er1.25, Zr5Er1.5 glasses in comparison with Zr5Er0 glass. The sharps of absorption spectra are identical, and the intensities of the glass samples are approximate the same height all the glass samples containing same concentration of ZrO_2, i.e., 5 mol%. The average of first absorption peak, the second absorption peak and the average of the apparent crystal field splitting value are 2227.24 ± 0.05 eV, 2230.27 ± 0.02 eV and 3.03 ± 0.05 eV, respectively. These parameters are very close to that of the standard reference (2227.20, 2230.27 and 3.07 eV) (Table 2). So, the XANES spectra can confirm that the oxidation state Zr atoms within all of glass samples is +4 and the sharp of spectra also indicates that Zr^{4+} ions are coordinated by six-fold oxygen. Thus, it can be implied that Er_2O_3 do not affect to the chemical environment around Zr^{4+} ions both the oxidation state and the coordination number.

In Er_2O_3 containing glasses, Er L_{III} XANES experiment is also performed. The Er L_{III} XANES spectra of glasses and Er_2O_3, which has the oxidation state to be equivalent to +3 show in Figure 8(a). The white line peak position of the Er L_{III}- edge of glass samples and the reference compound are nearly identical which an average of the absorption peaks of samples and reference compound are 8363.06 ± 0.14 eV and 8363.76 eV, respectively, as compared in (Table 3). The energy difference of the white line peak position is less than 0.8 eV. Thus, the XANES data can confirm that the oxidation state of Er ions in all of glass samples is equivalent to +3.

EXAFS in R-space of Zr5Er1 glass presents in Figure 8(b), when probing for Er atom.To investigate the local structure, Artemis program is utilized for fitting the experimental spectra to the crystal data from the Crystallographic Information File (CIF) to the experimental spectra. The crystal data of Er_2SiO_7 (monoclinic- P21/c) is selected to find the acceptable fitting parameter including S_0^2 (the amplitude reduction) in a range of 0.7 to 1.2, σ2 (Debye-Waller factors) higher than 0.003, ΔE_0 (an adjustment to the E_0) in a range of - 10 eV to 10 eV and R-factor (a statistical value referring to the difference between the model and experimental data) less than 0.05 [46].The fitting parameters of Zr5Er1 glass are shown in Table 4. All fitting parameters are in an acceptable range. The EXAFS results reveal crucial information about the chemical environment around Er^{3+} ion that is coordinated by six oxygen atoms. However, the fitted EXAFS spectra indicate an absence of full symmetry in the shape of the octahedral sites. The bond lengths between Er^{3+} and O^{2-} ions (Er-O) were found to be non-equivalent. The calculation performed using the Artemis software classifies radial distances between Er^{3+} and O^{2-}. The results can be classified oxygen atoms as 3 types depending on the Er-O distances, consisting of 2.209 Å (4 oxygens), 2.246 Å (1 oxygen), and 2.318 Å (1 oxygen), respectively.

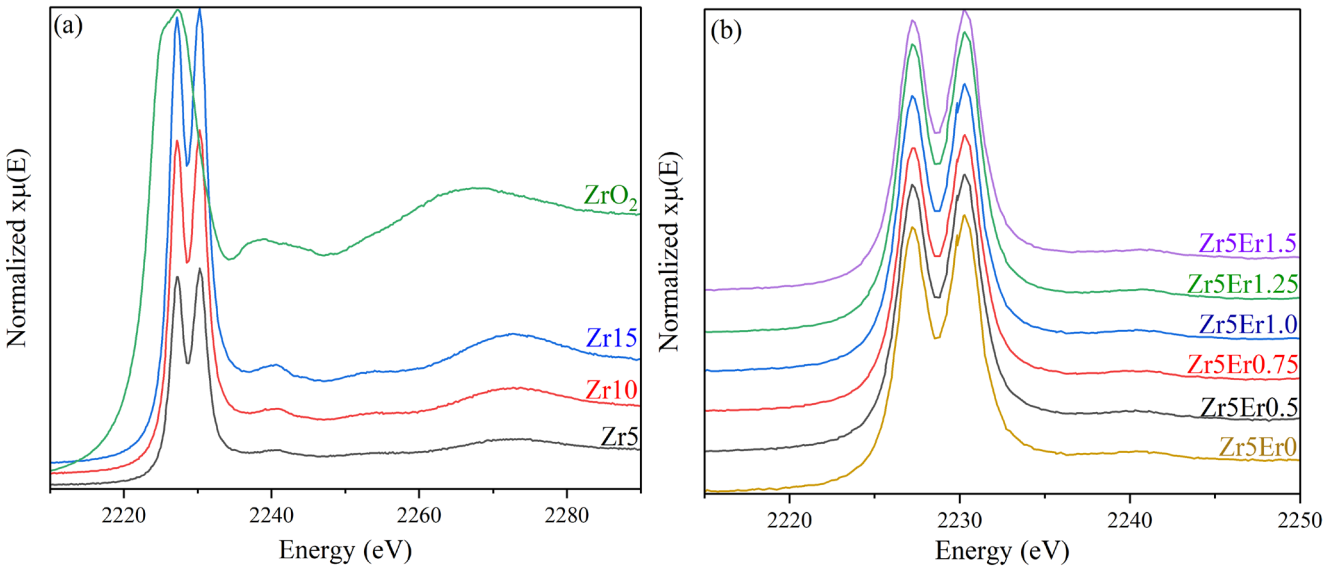

Figure 7. $Zr_{L\text{-}III}$ XANES spectra of (a) ZrO_2 standard and glasses containing different ZrO_2 concentrations, and (b) glasses containing different Er_2O_3 concentrations.

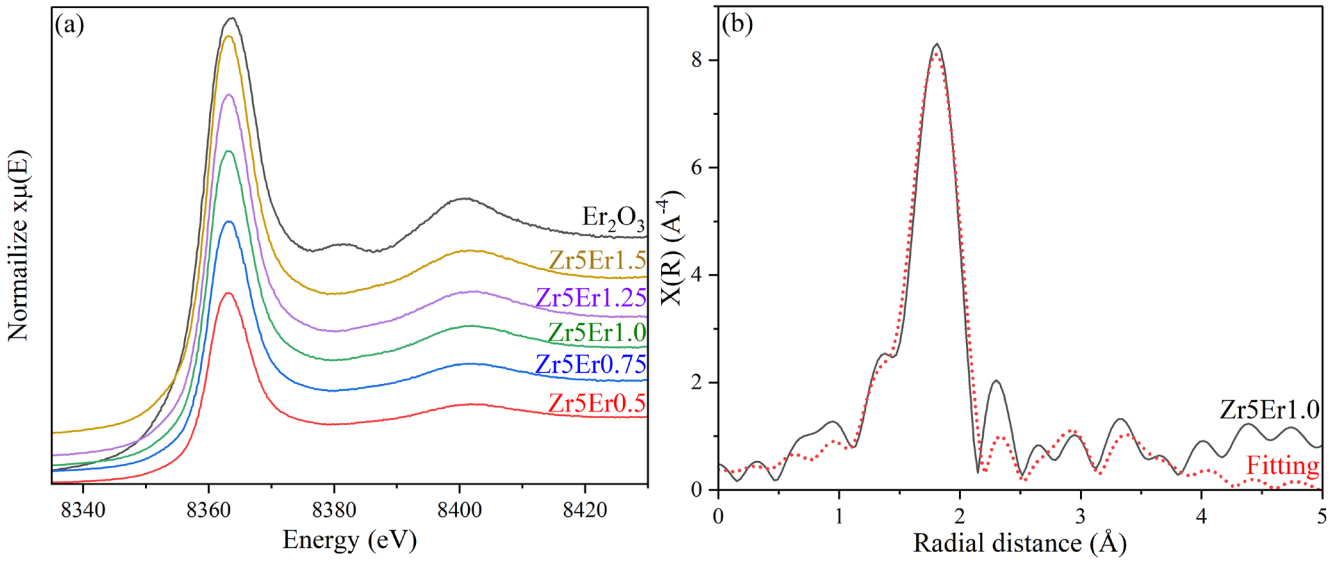

Figure 8. (a) $Er_{L\text{-}III}$ XANES spectra of glasses containing different Er_2O_3 concentrations and (b) $Er_{L\text{-}III}$ EXAFS spectra of Zr5Er1.

Table 2. The XANES parameters of Zr L_{III}-edge including the absorption peak and crystal field splitting value.

Samples	First absorption peak (eV)	Second absorption peak (eV)	Crystal field splitting value (eV)
ZrO_2	2227.29	-	-
Zr5	2227.20	2230.29	3.09
Zr10	2227.21	2230.28	3.07
Zr15	2227.21	2230.29	3.08
Zr5Er0	2227.20	2230.27	3.07
Zr5Er0.5	2227.20	2230.29	3.09
Zr5Er0.75	2227.34	2230.30	2.96
Zr5Er1.0	2227.22	2230.27	3.05
Zr5Er1.25	2227.22	2230.25	3.03
Zr5Er1.5	2227.23	2230.25	3.02

Table 3. The XANES absorption peak of Er L_{III}-edge.

Samples	Absorption edge (eV)
E_2O_3	8363.76
Zr5Er0.5	8362.95
Zr5Er0.75	8363.13
Zr5Er1.0	8362.92
Zr5Er1.25	8363.26
Zr5Er1.5	8363.05

Table 4 EXAFS fitting parameters of Er^{3+}including atomic distances (R), coordination numbers (N), Debye-Waller factors (σ^2), amplitude reduction (S_0^2), R-factor, and reduced chi-square.

Path	N	S_0^2	σ^2	E_0 (eV)	R (Å)	R-factor	Reduced chi-square
Er-O (1)	4	1.00	0.00536	0.935	2.20917		
Er-O (2)	1	1.00	0.00536	0.935	2.24607	0.016	41.70
Er-O (3)	1	1.00	0.00536	0.935	2.31850		

3.4 Density of glasses

The relationship of the densities and ZrO_2 concentrations is shown in Figure 9(a). It can be noticed that the density gradually increased from 2.54 g·cm^{-3} to 2.81 g·cm^{-3} when ZrO_2 concentrations increases. The increase in density refers to the difference between molecular weight of SiO_2 (60.08 g·mol^{-1}) and ZrO_2 (123.22 g·mol^{-1}). SiO_2 is replaced by ZrO_2 that has higher molecular weight. As a result, the average molecular weight of bulk glasses increases.

The relationship of the densities and Er_2O_3 concentration is shown in Figure 9(b). The density increases linearly with additional content of Er_2O_3 from 2.64 g·cm^{-3} to 2.82 g·cm^{-3}. The result indicates that replacing

Na_2O (61.98 g·mol^{-1}) with a small amount of Er_2O_3 (382.56 g·mol^{-1}) in the bulk glasses leads to an increase in their average molecular weight [47].

Figure 10 shows the molar volume incretion of doped glasses as a function of ZrO_2 and Er_2O_3 concentrations. As the concentration of ZrO_2 varies from 0 to 15 mol% (Figure 10(a)), the molar volume rises from 22.45 cm^3·mol^{-1} to 23.63 cm^3·mol^{-1}. In case of Er_2O_3, the molar volume dramatic changes from 22.75 cm^3·mol^{-1} to 23.02 cm^3·mol^{-1} even doped at a very low concentration as shown in Figure 10(b).

3.5 Microhardness of glasses

The relation between Vicker microhardness and ZrO_2 concentration is shown in Figure 11(a). The Vicker microhardness of Zr0, Zr5, Zr10 and Zr15 glasses are 582.12, 698.23, 787.38 and 802.82 HV, respectively. The results indicate the micro hardness increasing with increasing ZrO_2 concentration. The improve of Vicker microhardness has been explained by the increment of bond strength of the glass network and reduction of NBOs [48]. The Raman spectra reveals that ZrO_2 behaves as a glass former by bonding with $[SiO_4]^{4-}$ tetrahedral site via Si-O-Zr bonds which lead to increase of the average bond strength of the network. Furthermore, the intensity reduction of Q^3 (Na) peak at 1070 cm^{-1} compared to Q^3 (Ca) peak at 1030 cm^{-1} suggests that Na^+ ions are converted to charge compensators in order to eliminate excess negative charges near the $[ZrO_6]^{2-}$ units instead of network modifiers near the NBO sites. This conversion directly affects to the decrease of non-bridging oxygen [49]. As confirmed by XANES spectra, zirconium ions coordinate with six oxygen atoms, although its oxidation state retain as +4. This observation confirms excess negative charges surrounding $[ZrO_6]^{2-}$ units.

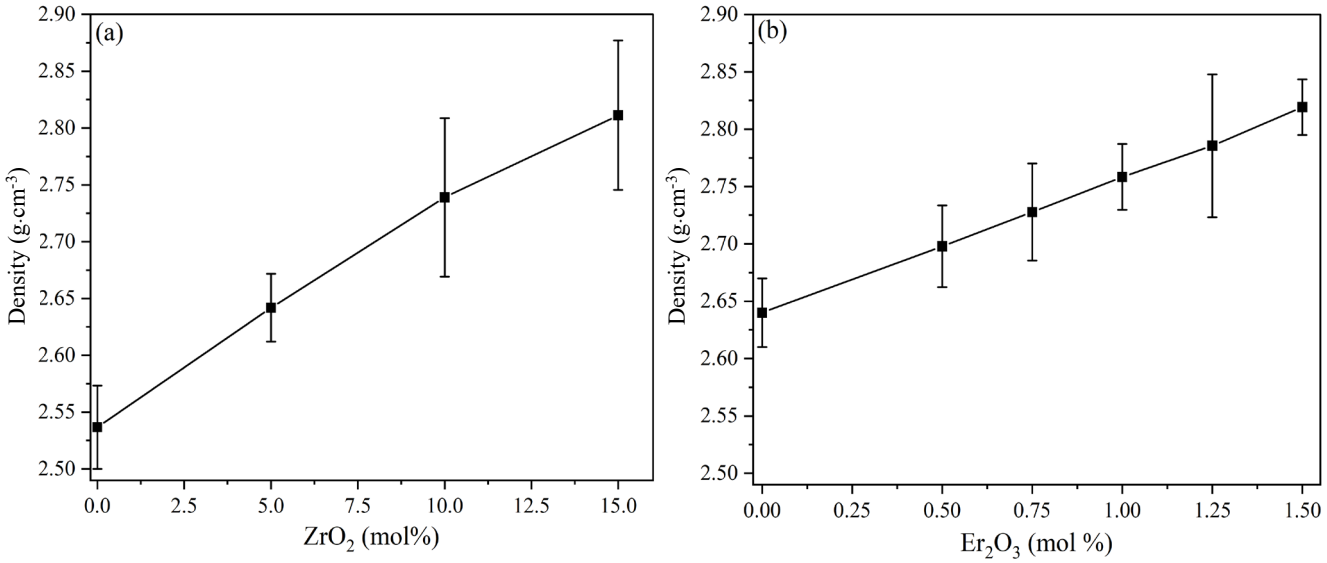

Figure 9. Bulk density of (a) glass containing different ZrO_2 concentrations and (b) glass containing different Er_2O_3 concentrations.

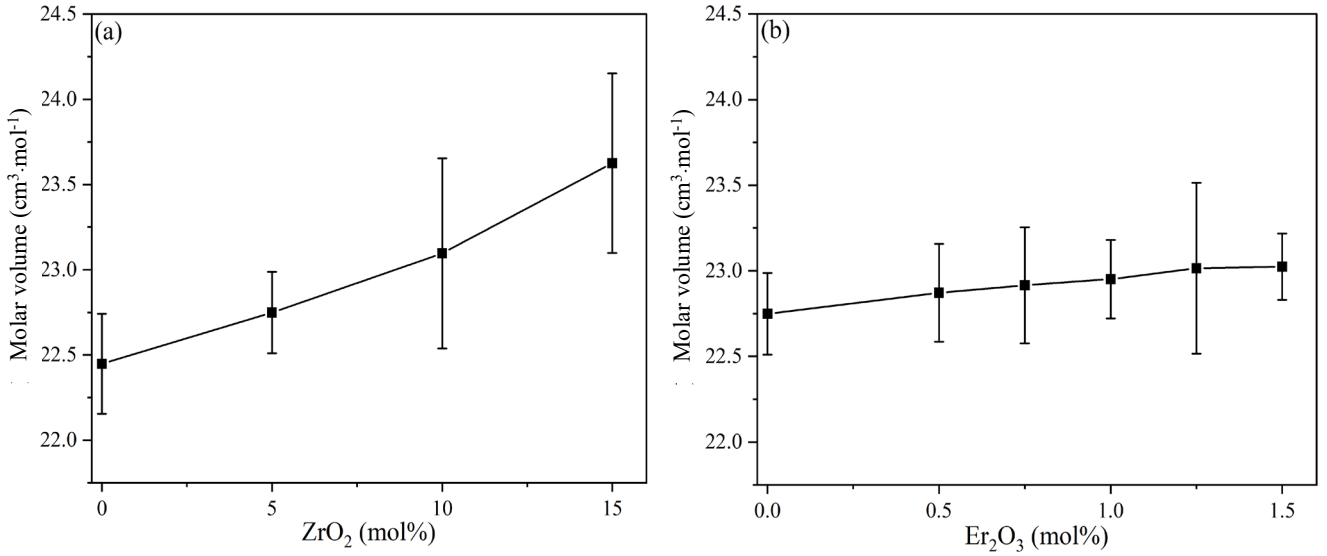

Figure 10. Changes in the molar volume of the glass samples at different concentrations of (a) ZrO_2 and (b) Er_2O_3.

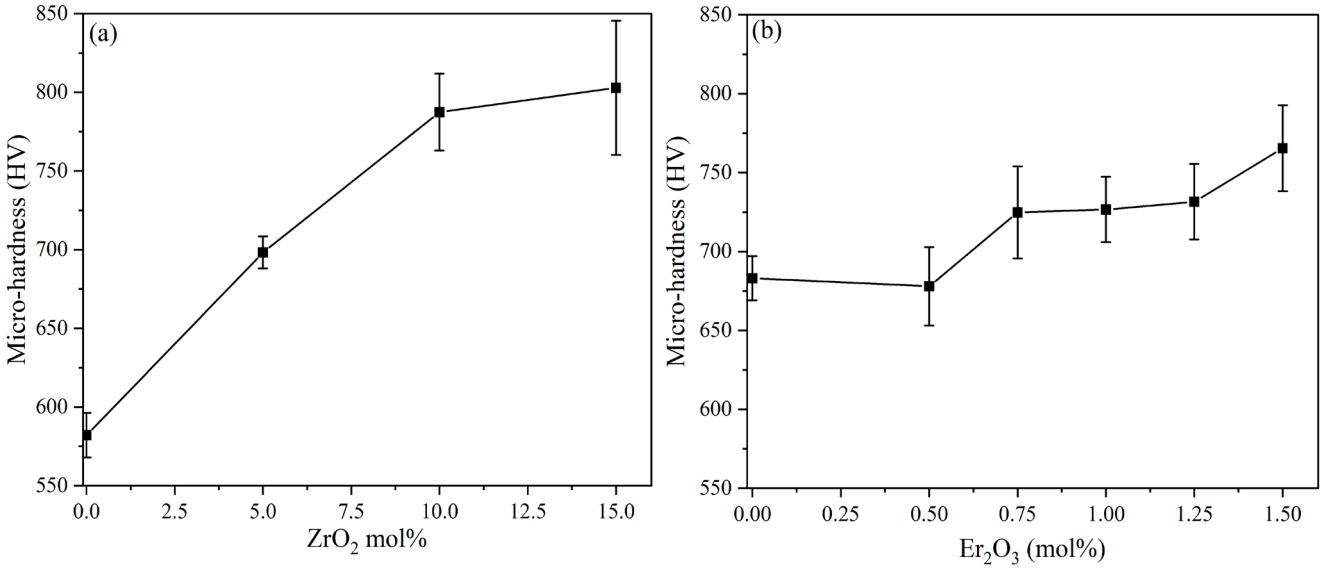

Figure 11. Micro-hardness of (a) glasses containing different ZrO_2 concentrations, and (b) glasses containing different Er_2O_3 concentrations.

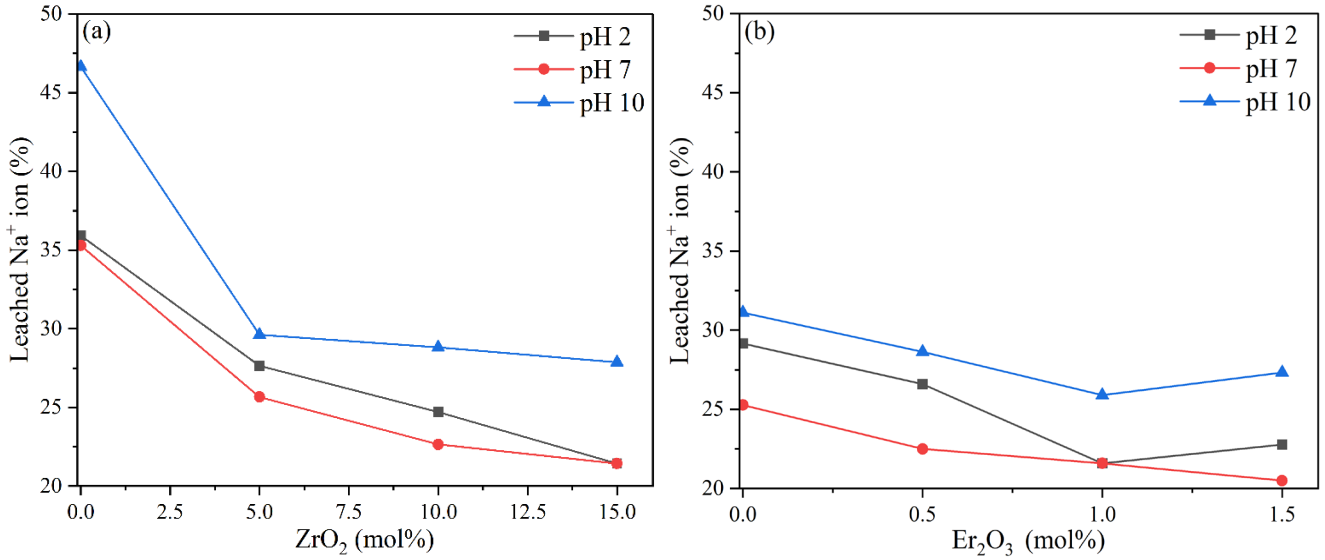

Figure 12. Percentage of leached Na^+ ions under acidic, neutral, and basic environments of (a) glasses containing different ZrO_2 concentrations, and (b) glasses containing different Er_2O_3 concentrations.

The Vicker microhardness of Zr5Er0, Zr5Er0.5, Zr5Er0.75, Zr5Er1.0, Zr5Er1.25, and Zr5Er1.5 glasses show in Figure 11(b). The trend of microhardness is higher when concentrations of Er_2O_3 increase from 698.23 HV to 765.36 HV, which is due to the increase of bond energy (cationic field strength) [23,49]. From the XAS and Raman spectroscopy studies, the results reveal that the role of Er^{3+} ion is as same as other alkali or alkali earth ions as the glass network modifier. However, Er-O bonds have higher bond energy than Na-O bonds (see Table 1). The bond energy of the network modifiers directly correlates with the strength of the glass network. A stronger network is more resistant to deformation and scratching. When Er^{3+} ions distribute to the glass structure, they interact with O^{2-} ions and hold more tightly leading to enhance the overall structural stability of the glass matrix.

3.6 Na^+ ion leaching

The percentages of Na^+ ions leached from glass samples under acidic (pH 2), neutral (pH 7) and basic (pH 10) environment are shown in Figure 12(a). In the case of Zr0 glass, the percentages of leached Na^+ ions are 35.92, 35.28, and 46.65% depending on the environmental solutions. Basic environment has the highest ability to extract Na^+ ions from the glass network into the solution. For ZrO_2 containing glasses, the percentage of Na^+ ions in solution decreases as a function of concentration of ZrO_2. In basic solution, the percentage of leached Na^+ ions reduce from that of Zr0 to 29.61%, 28.82%, and 27.87% for 5, 10 and 15% mol ZrO_2, respectively. In addition, for the case of immersion in acid solution, the percentages of leached

Na^+ ions decrease from that of Zr0 to 27.64, 24.70, and 21.44% for 5, 10 and 15% mol ZrO_2, respectively. Finally, for neutral solution, the percentages of leached Na^+ ions decrease from that of Zr0 to 25.66, 22.65, and 21.43% for 5, 10 and 15% mol ZrO_2, respectively.

The leaching process can be explained by the ion-exchange mechanism describing the process as interdiffusion of cations such as Na^+ and H^+ ions through the structure of bulk glass [4,5,50]. This process is regarding cations, acting as network modifier at NBO sites, to be removed from the surface and then to be replaced by H^+ ion. Hence, the total number of NBO sites and types of the network modifier are crucial parameters controlling the leaching rate. The results from Zr L_{III} XANES spectra and Raman spectra confirm that the Zr-octahedral site ($[ZrO_6]^{2-}$) can generate the negative charge surplus. To balance the negative charge surplus, some of Na^+ ions to be transformed from network modifier role to charged compensator role. Na^+ ions performing as the charge compensator have been reported that they are approximately five orders of magnitude more resistant to ion-exchange by H^+ ion than the network modifier (≡Si-O-Na) [50]. As a result, the amount of leached Na^+ ions decrease significantly.

The percentages of leached Na^+ ions of Zr5Er0, Zr5Er0.5, Zr5Er0.75, Zr5Er1.0, Zr5Er1.25, and Zr5Er1.5 glasses demonstrate in Figure 12(b). In basic solution, the percentage of leached Na^+ ions gradually decreases from 31.10 to a range 28.63% to 25.90% when amount of Er_2O_3 is added. It should be pointed out that glass in the basic solution still has the highest potential to extract Na^+ ions from glass structure compared with acidic and basic solution. This is supported by the fact that hydroxyl ions (OH^-), from the basic solution, destroy the siloxane bonds (Si-O-Si), acting as backbone of the glass network (Equation (4)). After that, surface of glass is deformed to a more open "gel-like" structure [5,50]. As a result, the leaching process can occur not only on the glass surface, but also inside the glass matrix.

$$\equiv Si\text{-}O\text{-}Si\equiv + OH^- \rightarrow \equiv Si\text{-}OH + \equiv Si\text{-}O^- \qquad (4)$$

The percentages of leached Na^+ ions from glass sample in acid solution decrease from 29.16% to a range of 26.58% to 21.58% and the value is still higher than in neutral condition due to within the solution having much more H^+ ion as a source for the ion-exchange process. The percentages of leached Na^+ ions from glass sample in neutral solution decrease from 25.27 to a range of 22.49% to 20.48% which the trend is the same as acidic and basic solution. From Na^+ ions leaching experiment, it is obvious that ZrO_2 and Er_2O_3 are effective dopants for reducing the leaching of Na^+ ions. For comparison, Er_2O_3 has more than 10 times stronger effect even doped at a very low amount (Figure 12).

The results indicate that Er_2O_3 can reduce the amount of leached Na^+ ions. Although, the Raman spectra reveal that Er^{3+} ions act as the network modifier and increases NBO species, especially Q^1 unit. The XANES and EXAFS data show the converse results which confirm that the oxidation number of Er^{3+} ions less than the coordination number. It suggests that Er^{3+} ions are not only acting as modifier with $[SiO^4]^{4-}$ unit but also behaving as a negative polyhedral site absorbing Na^+ ions to rebalance the negative charge surplus. Therefore, some NBO sites are removed. Furthermore, the bond energy of the Er^{3+} ions is higher than alkali and alkali earth cation (Table 3) inducing strong bonding between Er^{3+} and neighboring O^{2-} ions which can enhance network rigidity of glass system [51]. According to mixed-cation effect, the less mobile Er^{3+} ions also occupy large interstitial site in the glass network being able to block the diffusion of Na^+ and H^+ ions. For these reasons, the ion-exchange rate between alkali cation and H^+ ion is retarded.

4. Conclusions

The local structures and roles of zirconium and erbium ions in $10Li_2O$-(15-y)Na_2O-10CaO-(65-x)SiO_2-xZrO_2-y-Er_2O_3 glasses were studied by Raman spectrometer and XAS. The ZrO_2 in the glass structure acts as glass network former as well as silicon, forming $[ZrO_6]^{2-}$ octahedra connected to the silicate network via Zr-O-Si bonds and induces the formation of Q^4 (Zr,Zr) units together with reduction the proportion of NBOs. In the case of Er_2O_3, two assumptions were proposed. The first is that the addition of the rare-earth cations acts as a modifier in the $[SiO_4]^{4-}$ tetrahedral sites, decreasing the degree of connectivity and increasing the concentration of NBOs. The second assumption is that the shift in peak position to lower frequency is due to the change in the symmetric stretching frequency of the $[SiO_4]^{4-}$ tetrahedra when NBO bonds with Er^{3+} ions. Density and Vicker microhardness of modified glasses increased as the concentration of ZrO_2 and Er_2O_3 increased. In this work, the leaching of Na^+ ions from the obtained glasses can be explained by an ion-exchange mechanism involving the interdiffusion of cations through the glass structure. Adding ZrO_2 to the alkali silicate glass can decrease the amount of leached Na^+ ions in solution, with the greatest decrease observed in basic solution. The Zr^{4+} ions are presented in the form of octahedral environment ($[ZrO_6]^{2-}$). The negative charge surplus of $[ZrO_6]^{2-}$, causes some Na^+ ions to transform from a network modifier to a charge compensator, making them more resistant to ion-exchange by hydrogen ions. Moreover, adding Er_2O_3 to the alkali silicate glass can also decrease the amount of leached Na^+ ions, despite increasing the number of NBO species. This is because Er^{3+} ions affect to increase bond energy and act as negative polyhedral sites that absorbs Na^+ ions to balance the negative charge surplus, leading to the removal of some NBO sites. The reduction of Na^+ ion leaching is due to high degree of connectivity of glass network and the transformation of Na^+ ions from network modifier to charge compensator.

Acknowledgements

We would like to express the profound gratitude to Synchrotron Light Research Institute (Public Organization), Thailand for the XAS instrument support (BL 5.2). Additionally, we are grateful to Teaching Assistant and Research Assistant (TA&RA) Scholarships from Graduate School, Chiang Mai University, Thailand for financial support.

References

[1] N. Mascaraque, M. Bauchy, and M. Smedskjaer, "Correlating the network topology of oxide glasses with their chemical durability," *The Journal of Physical Chemistry B*, vol. 121, no. 5, pp. 1139-1147, 2017.

[2] M. D. Bardi, H. Hutter, M. Schreiner, and R. Bertoncello, "Potash-lime-silica glass: protection from weathering," *Heritage Science,* vol. 3, no. 22, pp. 1-9, 2012.

[3] W. Deng, J. Cheng, P. Tian, and M. Wang, "Chemical durability and weathering resistance of canasite based glass and glass-ceramics," *Journal of Non-Crystalline Solids,* vol. 358, no. 21, pp. 2847-2854, 2012.

[4] E. Meechoowas, P. Jampeerung, K. Tapasa, U. Pantulap, and T. Jitwatcharakomol, "Glass batch modification to improve the weathering resistance in soda-lime silicate glass," *Key Engineering Materials,* vol. 798, pp. 206-211, 2019.

[5] A. K. Varshneya, and J. C. Mauro, Fundamentals of Inorganic Glasses, Amsterdam: Elsevier Inc, 2019.

[6] R. Makhlouk, Z. Chabbou, Y. Er-rouissi, M. Taibi, and S. Aqdim, "Chemical durability, Properties and structural approach of the glass series xFe_2O_3-(45-x) PbO-$55P_2O_5$ (with $0 \leq x \leq 20$; mol%)," *New Journal of Glass and Ceramics,* vol. 13, pp. 1-16, 2023.

[7] J. Zhao, Y. Wang, J. Kang, Y. Qu, G. Khater, S. Lia, Q. Shia, and Y. Yue, "Effect of SnO_2 on the structure and chemical durability of the glass prepared by red mud," *Journal of Non-Crystalline Solids,* vol. 509, pp. 54-59, 2019.

[8] S. Li, Y. Lu, Y. Qua, Y. Xu, L. Ming, Z. Song, and Y. Yue, "Influences of ZnO on the chemical durability and thermal stability of calcium iron phosphate glasses," *Journal of Non-Crystalline Solids,* vol. 498, pp. 228-235, 2018.

[9] L. Xiongwei, L. Mei, W. Mitang, L. Zhaogang, H. Yanhong, and T. Junhu, "Effects of neodymium and gadolinium on weathering resistance of ZnO-B_2O_3-SiO_2 glass," *Journal of Rare Earths,* vol. 32, no. 9, pp. 874-878, 2014.

[10] T. Poungkaew, M. Jaimasith, P. Leowkijsiri, and W. Thiemsorn, "Industrial soda-lime-silica sheet glass hardened by zirconia-reinforced inorganic coating," *TNI Journal of Engineering and Technology,* vol. 2, no. 1, pp. 6-10, 2014.

[11] J. Fisher, P. James, and J. Parker, "Soda lime zirconia silicate glasses as prospective hosts for zirconia-containing radioactive wastes," *Journal of Non-Crystalline Solids,* vol. 351, no. 8-9, pp. 623-631, 2005.

[12] I. Hussain, E. K. Barimah, Y. Iqbal, G. Jose, A. Zeb, and R. Muhammad, "Mechanical and optical properties of ZrO_2 doped silicate glass ceramics," *Silicon,* vol. 13, pp. 877-883, 2021.

[13] M. Lobanova, A. Ledieu, P. Barboux, F. Devreux, O. Spalla, and J. Lambard, "Effect of ZrO_2 on the glass durability Materials," *Research Society,* vol. 713, no. 151, pp. 1-9, 2002.

[14] C. Cailleteau, F. Algeli, F. Devreux, S. Gin, J. Jestin, P. Jollivet, and O. Spalla, "Insight into silicate-glass corrosion mechanisms," *Nature Materials,* vol. 7, pp. 978-983, 2008.

[15] A. Quintas, D. Caurant, O. Majerus, P. Loiseau, T. Charpentier, and J. Dussossoy, "ZrO_2 addition in soda-lime aluminoborosilicate glasses containing rare earths: Impact on the network structure," *Journal of Alloys and Compounds,* vol. 714, pp. 47-62, 2017.

[16] L. Cormier, O. Dargaud, G. Calas, C. Jousseaume, and S. Papin, "Zr environment and nucleation role in aluminosilicate glasses," *Materials Chemistry and Physics,* vol. 152, pp. 41-47, 2015.

[17] P. Jollivet, G. Calas, L. Galoisy, F. Angeli, B. Bergeron, S. Gin, M. Ruffoni, and N. Trcera, "An enhanced resolution of the structural environment of zirconium in borosilicate glasses," *Journal of Non-Crystalline Solids,* vol. 381, pp. 40-47, 2013.

[18] X. Lu, L. Deng, S. Kerisit, and J. Du, "Structural role of ZrO_2 and its impact on properties of boroaluminosilicate nuclear waste glasses," *npj Materials Degradation,* vol. 2, no. 19, pp. 1-10, 2018.

[19] F. Angeli, F. T. Charpentier, D. Ligny, and C. Cailleteau, "Boron speciation in soda lime borosilicate glasses containing zirconium," *Journal of the American Ceramic Society,* vol. 93, no. 9, pp. 2693-2704, 2010.

[20] Z. Wang, and L. Cheng, "Effects of doping CeO_2/TiO_2 on structure and properties of silicate glass," *Journal of Alloys and Compounds,* vol. 597, pp. 167-174, 2014.

[21] F. Lofaj, R. Satet, M. Hoffmann, F. Dorčáková, and A. R. D. A. López, "Rheological properties of the rare-earth doped glasses," *Key Engineering Materials,* Vols. 264-268, pp. 1867-1870, 2004.

[22] A. V. Deepa, P. Vinothkumar, K. S. Moorthy, P. Muralimanohar, M. Mohapatra, S. Praveenkumar, and P. Murugasen, "Optical, electrical, mechanical properties of Pr^{3+} and Yb^{3+} doped phosphate glasses," *Optical and Quantum Electronics,* vol. 52, no. 11, pp. 1-28, 2020.

[23] F. Lofaj, P. Hvizdos, F. Dorc˘a´kova´, R. Satet, M. J. Hoffmann, and A. R. D. Arellano-Lo´pez, "Indentation moduli and micro-hardness of RE-Si-Mg-O-N glasses (RE=Sc, Y, La, Sm, Yb and Lu) with different nitrogen content," *Materials Science and Engineering,* vol. 357, no. 1-2, pp. 181-187, 2003.

[24] P. P. Puga, P. Danyliuk, A. I. Gomonai, H. V. Rizak, I. M. Rizak, V. M. Rizak, G. D. Puga, L. Kvetková, and M. M. Byrov, "Raman scattering in glassy $Li_2B_4O_7$ doped with Er_2O_3," *Ukrainian Journal of Physical Optics,* vol. 19, no. 4, pp. 211-219, 2018.

[25] O. Majérus, D. Caurant, A. Quintas, J. Dussossoy, I. Bardez, and P. Loiseau, "Effect of boron oxide addition on the Nd^{3+} environment in a Nd-rich soda-lime aluminoborosilicate glass," *Journal of Non-Crystalline Solids,* vol. 357, no. 14, pp. 2744-2751, 2011.

[26] M. Wang, J. Cheng, M. Li, and F. He, "Raman spectra of soda–lime–silicate glass doped with rare earth," *Physica B,* vol. 406, no. 20, pp. 3865-3869, 2011.

[27] D. Caurant, P. Loiseau, O. Majérus, V. A. Chevaldonnet, I. Bardez, and A. Quintas, Glasses, glass-ceramics and ceramics for immobilization of highly radioactive nuclear, New York: Nova Science Publishers, Inc., 2009.

[28] A. Quintas, D. Caurant, O. Majerus, P. Loiseau, T. Charpentier, and J. Dussossoy, "ZrO_2 addition in soda-lime aluminoborosilicate glasses containing rare earths: Impact on rare earths environment and crystallization," *Journal of Alloys and Compounds,* vol. 719, pp. 383-397, 2017.

[29] M. Wang, J. Cheng, Q. Liu, P. Tian, and M. Li, "The effect of light rare earths on the chemical durability and weathering of Na_2O–CaO–SiO_2 glasses," *Journal of Nuclear Materials,* vol. 400, no. 2, pp. 107-111, 2010.

[30] R. M. Almeida, and L. F. Santos, "Raman spectroscopy of glasses," in *Modern Glass Characterization*, Ed. Hoboken, Wiley-American Ceramic Society, 2015, pp. 74-106.

[31] M. F. Dilmore, D. E. Clark, and L. L. Hence, "Chemical durability of Na_2O-K_2O-CaO-SiO_2 glasses," *Journal of the American Ceramic Society,* vol. 61, no. 9-10, pp. 439-443, 2006.

[32] D. R. Neuville, "Viscosity, structure and mixing in (Ca, Na) silicate melts," *Chemical Geology,* vol. 229, no. 1-3, pp. 28-41, 2006.

[33] T. Furukawa, K. E. Fox, and W. B. White, "Raman spectroscopic investigation of the structure of silicate glasses. III. Raman intensities and structural units in sodium silicate glasses," *The Journal of Chemical Physics,* vol. 75, pp. 3226-3237, 1981.

[34] K. Fukumi, J. Hayakawa, and T. Komiyama, "Intensity of Raman band in silicate glasses," *Journal of Non-Crystalline Solids,* vol. 119, no. 3, pp. 297-302, 1990.

[35] A. K. Yadav, and P. Singh, "A review of the structures of oxide glasses by Raman spectroscopy," *RSC Advances,* vol. 5, pp. 67583-67609, 2015.

[36] M. Ficheux, E. Burov, G. Aquilanti, N. Trcera, V. Montouillout, and L. Cormier, "Structural evolution of high zirconia alumino-silicate glasses," *Journal of Non-Crystalline Solids,* vol. 539, pp. 1-11, 2020.

[37] J. S. McCloy, J. Marcial, D. Patil, M. Saleh, M. Ahmadzadeh, H. Chen, J. V. Crum, B. J. Riley, H. Kamat, A. Bréhault, A. Goel, K. E. Barnsley, J. V. Hanna, P. Rajbhandari, and C. L. Corkhill, "Glass structure and crystallization in boro-alumino-silicate glasses containing rare earth and transition metal cations," *MRS Advances ,* vol. 4, p. 1029-1043, 2019.

[38] N. Chouard, D. Caurant, O. Majérus, J. L. Dussossoy, S. Klimin, D. Pytalev, R. Baddour-Hadjean, and J. P. Pereira-Ramos, "Effect of MoO_3, Nd_2O_3, and RuO2 on the crystallization of soda–lime aluminoborosilicate glasses," *Journal of Materials Science,* vol. 50, p. 219-241, 2015.

[39] G. E. Brown, F. Farges, and G. Calas, "X-ray scattering and X-ray spectroscopy studies of silicate melts," *Reviews in Mineralogy and Geochemistry,* vol. 32, pp. 317-410, 1995.

[40] J. Du, and A. N. Cormack, "The structure of erbium doped sodium silicate glasses," *Journal of Non-Crystalline Solids,* vol. 351, no. 27-29, pp. 2263-2276, 2005.

[41] L. Robinet, D. Neff, A. Bouquillon, S. P. Camagna, and A. V. Carron, "Raman spectroscopy, a non-destructive solution to the study of glass and its alteration," in *ICOM 15th triennial conference*, New Delhi, 2008.

[42] A. J. G. Ellison, and P. C. Hess, "Lanthanides in silicate glasses: A vibrational spectroscopic study," *Journal of Geophysical Research: Solid Earth,* vol. 95, no. B10, pp. 15,717-15,726, 1990.

[43] A. J. G. Ellison, and P. C. Hess, "Vibrational spectra of high-silica glasses of the system K_2O-SiO_2-La_2O_3," *Journal of Non-Crystalline Solids,* vol. 127, no. 3, pp. 247-258, 1991.

[44] R. B. Greegor, K. Y. Blohowiak, J. H. Osborne, K. A. Krienke, and J. T. Cherian, "X-ray spectroscopic investigation of the Zr-site in thin film sol-gel surface preparations," *Journal of Sol-Gel Science and Technology,* vol. 20, pp. 35-50, 2001.

[45] L. Cormier, O. Dargaud, G. Calas, C. Jousseaume, S. Papin, N. Trcera, and A. Cognigni, "Zr environment in alumino-silicate glasses Zr environment and nucleation role in alumino-silicate glasses," *Materials Chemistry and Physics,* vol. 152, pp. 41-47, 2015.

[46] K. Samkongngam, "Spectroscopic studies of transition metal ions in silicate glass," Bangkok, 2019.

[47] W. Kaewwiset, K. Thamaphat, J. Kaewkhao, and P. Limsuwan, "Er^{3+}-doped soda-lime silicate glass: artificial pink gemstone," *American Journal of Applied Sciences,* vol. 11, pp. 1769-1775, 2012.

[48] Y. Lin, M. M. Smedskjaer, and J. C. Mauro, "Structure, properties, and fabrication of calcium aluminate-based glasses," *The International Journal of Applied Glass Science,* vol. 10, pp. 488-501, 2019.

[49] K. Januchta, M. Bauchy, R. E. Youngman, S. J. Rzoska, M. Bockowski, and M. M. Smedskjaer, "Modifier field strength effects on densification behavior and mechanical properties of alkali aluminoborate glasses," *Physical Review Materials,* vol. 1, no. 6, pp. 1-12, 2017.

[50] B. C. Bunker, "Molecular mechanisms for corrosion of silica and silicate glasses," *Journal of Non-Crystalline Solids,* vol. 179, pp. 300-308, 1994.

[51] M. Kim, C. L. Corkhill, N. C. Hyatt, and J. Heo, "Development, characterization and dissolution behavior of calcium-aluminoborate glass wasteforms to immobilize rare-earth oxides," *Scientific Reports,* vol. 8, pp. 1-8, 2018.